DOI 10.24425/aee.2024.148866

Optimal configuration of energy storage system capacity in traction power supply system considering photovoltaic consumption

WEI ZHANG ✉, XIAOQIANG CHEN, YING WANG

School of Automation and Electrical Engineering, Lanzhou Jiaotong University
Lanzhou,730070 China
e-mail: ✉ *wayzhang0108@163.com*

(Received: 25.09.2023, revised: 28.02.2024)

Abstract: In order to achieve energy savings and promote on-site integration of photovoltaic energy in electrified railways, a topology structure is proposed for the integration of photovoltaic (PV) and the energy storage system (ESS) into the traction power supply system (TPSS) based on a railway power conditioner (RPC). This paper analyzes the composition and operation principles of this structure. To assess the economic benefits brought by the integration of photovoltaic and energy storage systems, a bilevel optimization model is established, with the objectives of optimizing energy storage capacity configuration and photovoltaic energy integration. The KKT (Karush–Kuhn–Tucker) method is employed to transform the model into a single-layer mixed-integer linear programming model, which is then solved using the CPLEX solver in MATLAB. The research findings indicate that, with the configuration of the ESS, the optimal PV consumption rate achieved is 96.8749%. Compared to a 100% PV consumption rate, the ESS capacity configuration is reduced by 13.14%, and the overall operational cost of the TPSS is at its lowest. The study suggests that the proposed bilevel optimization algorithm can more effectively consider PV consumption, leading to enhanced economic performance of the TPSS operation.

Key words: bilevel optimization, capacity optimization configuration, energy storage system, photovoltaic, railway power conditioner, traction power supply system

1. Introduction

In the year 2022, the operational railway mileage in China reached 155 000 kilometers, among which the operational mileage of high-speed railways reached 42 000 kilometers, with a double-track rate of 59.6% and an electrification rate of 73.8%. The operational railway mileage in the western regions amounted to 63 000 kilometers. The national railway sector's energy

consumption was equivalent to 15.1258 million tons of standard coal [1]. The rapid advancement of high-speed railways has not only facilitated convenient transportation for people, but has also drawn widespread attention to the substantial issue of energy consumption it entails.

Due to urgent demand for clean and renewable energy sources, research and application of renewable energy are actively being promoted worldwide. Reference [2] uses artificial intelligence methods to verify that photovoltaic (PV) systems serve as local power plants for each building, which can meet the internal energy needs of the building and an effective strategy for managing grid demand peaks. Reference [3] predicted the final balance of energy production and consumption for each building and the entire community as a microgrid in a community of buildings with solar panels and electric vehicles through a comparative study of machine learning and deep learning methods. Reference [4] explores the use of hybrid systems in wind farms integrating alkaline electrolyzers and hydrogen storage tanks with proton exchange membrane fuel cells to improve wind turbine performance. Reference [5] investigated the optimal utilization of renewable resources such as solar and wind energy in smart systems for residential buildings in Iran, emphasizing the use of artificial intelligence methods to accurately determine renewable energy production considering the large initial capital investment and economic feasibility system capacity. Electrified railways, being the largest individual load on the power grid, have seen electricity expenses become one of the primary operational expenditures. However, the current traction power supply system (TPSS) mainly draws power from the public grid. On the one hand, long-distance transmission in remote areas has resulted in significant energy losses. On the other hand, there is a substantial amount of renewable energy distributed along the railway lines. The TPSS has not capitalized on the geographical advantage of utilizing nearby renewable energy sources [6]. Electrified railways, coincidentally, offer favorable conditions for the integration and proximity-based absorption of PV power generation [7]. Germany's railway system has witnessed cases of megawatt-level PV energy integration, [8] delves into two existing approaches for integration: PV integrated into sound-absorbing walls, and the technical challenges associated with establishing PV power stations along railway lines and integrating them into the TPSS. In Japan, railways have effectively harnessed PV energy by installing PV systems on the roofs of train station platforms. [9] discusses the potential, features, and prospects of PV power generation systems on train station platform roofs. In existing engineering cases, the integration of PV into railways is more concentrated in the non-traction power supply domain, which has relatively lower technical difficulty and fewer issues with power quality. On the other hand, research on PV integration into the AC traction power supply domain is currently in the theoretical stage, and there are limited engineering cases available.

By directly connecting the PV to the supply arm through a single-phase inverter, [10] has achieved on-site access and consumption of PV power sources along the railway without affecting the original structure of the TPSS. This method has the advantages of low investment cost and short construction period. However, it overlooks power quality issues such as negative sequence, harmonics, etc. Railway power conditioner (RPC) is typically utilized to enhance the power quality performance of electrified railway systems. It possesses the capability to balance negative sequence, suppress harmonic distortions, and compensate for reactive power, among other functions [11, 12]. By establishing a small-signal impedance model of the PV-train-grid coupled system and conducting an analysis, a novel extended forbidden region-based criterion was proposed [13]. This criterion was utilized to examine the impact of system parameters, including the RPC controller parameters, on low-frequency stability. Based on the energy storage type RPC

structure, a hierarchical optimization approach is introduced to address the challenges of negative sequence compensation and regenerative braking energy utilization in electrified railways [14]. Reference [15] proposes a train uninterrupted phase-separation passing system based on the energy storage type RPC, achieving constant power during the entire process of train passing phase separation and effectively avoiding electric power separation problems caused by the deceleration of trains on uphill sections of long ramp roads. Some have proposed the incorporation of PV and the energy storage system (ESS) at the intermediate DC link of the RPC, intending to employ it as a PV power generation system for traction purposes in railways [16]. By facilitating mutual coordination among subsystems, this approach aims to achieve the proximity-based absorption of PV energy and simultaneously accomplish power quality compensation. Research [17] indicates that the utilization efficiency of PV can be improved by integrating PV and the ESS into the TPSS through the choice of the RPC topology. This approach also allows for the recovery of regenerated braking energy from trains and enhances the quality of electrical energy in the TPSS. In the realm of optimization and configuration research, [18] introduces a hybrid energy storage system based on supercapacitors and lithium-ion batteries, along with an optimization configuration methodology. This approach employs mixed-integer linear programming to seek the optimal solution with the primary objective of minimizing costs. [19] established an economic optimization model for the entire life cycle of the electrified railway hybrid energy storage system, with the objective of maximizing the net profit throughout the system's life cycle. The improved particle swarm optimization algorithm was employed for solution finding. [20] has proposed an optimization configuration method that takes into account the overall economic performance level, utilizing an improved simulated annealing algorithm based on Levy flights to solve the capacity optimization configuration of hybrid energy storage systems. [21] proposed a bilevel model with the objective of minimizing the overall cost, comprising investment cost, replacement cost, operational cost, and electricity cost. The Sparrow Search Algorithm (SSA) with embedded CPLEX solver was employed to solve this two-tier nonlinear model. In summary, existing research in this area either focuses on non-traction electrical systems, does not take into account the utilization of renewable energy sources, or employs swarm intelligence algorithms, which can result in complex programming and slower solution speeds.

This paper utilizes the topology that integrates PV and the ESS into the TPSS through RPC, and categorizes the operational modes of the system into four forms. On the premise of rational abandonment of surplus PV energy, a bilevel optimization model is established to minimize the overall operational cost of the TPSS, with ESS capacity being configured within a reasonable range, thereby facilitating on-site consumption of PV power. Finally, the measured load data is used as input parameter solution to verify the feasibility and effectiveness of the proposed model.

2. System topology and operating mode

2.1. Topology

The topology of PV-ESS integration into the TPSS is illustrated in Fig. 1. The system consists of the TPSS, high-speed train, RPC, and a multi-source subsystem consisting of PV and the ESS.

The RPC consists of step-down transformers T_α and T_β, a set of back-to-back voltage source converters (VSC$_\alpha$ and VSC$_\beta$), and an intermediate DC-side capacitor C. The high-voltage sides of

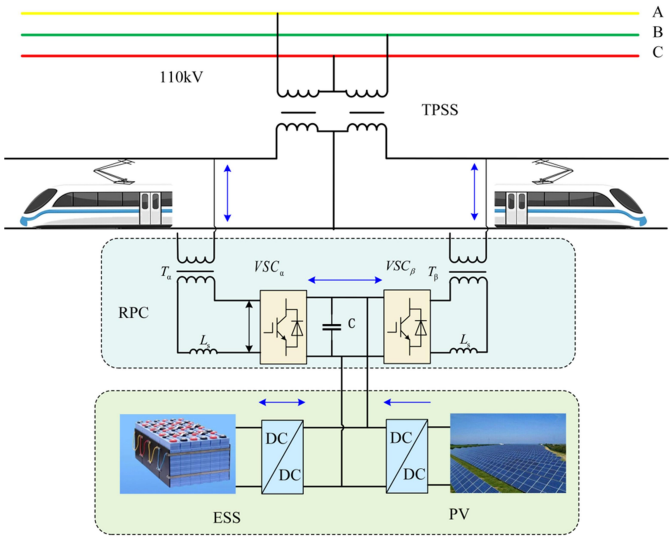

Fig. 1. Topology of PV and ESS integrated into the TPSS via RPC

the two step-down transformers, T_α and T_β, are connected to the α and β supply arms of the TPSS, while their low-voltage sides are connected to the two converters, serving as step-down isolators. Depending on the operational conditions, the two converters can operate either in rectification or inversion modes.

The PV system first achieves boost and maximum power point tracking through a DC/DC converter. The back-to-back converter is then utilized to dynamically distribute the PV energy. After filtering, the energy is connected to both sides of the 27.5 kV traction bus through a step-down transformer, along with the existing TPSS, jointly providing power to the TPSS. The ESS is connected to the DC link of the RPC through a bidirectional DC/DC converter, which controls the charging and discharging to balance the supply-demand difference between generation and load. In this structure, the left and right power arms share a set of the ESS through the RPC.

By coordinating and controlling the operational states of the multi-source subsystems, the system can achieve dynamic allocation of PV energy and comprehensive compensation for reactive power on the traction side, including periods when the PV system is generating power and when it is not. This configuration allows the system to meet the dual requirements of efficient consumption of PV energy and comprehensive power quality compensation.

This study focuses on utilizing the PV generation system as the primary source of electrical energy, supplemented by an ESS consisting of batteries. By improving the utilization of the PV energy and mitigating power fluctuations, the overall economic benefits of the system can be enhanced.

2.2. Operating mode

Let $P_{\mathrm{c\,max}}$ and $P_{\mathrm{d\,max}}$ represent the maximum charging and discharging power of the battery, $P_{\mathrm{pv\,max}}$ denotes the maximum output power of the PV system, $\mathrm{SOC}_{\max}$ and $\mathrm{SOC}_{\min}$ represent the upper and lower limits of the ESS's state of charge (SOC). The SOC is utilized to gauge the residual

capacity of the ESS, it denotes the proportion of the present remaining charge in comparison to its rated charge capacity. P_{pv} is indicating the output power of the PV system, P_{bat} representing the power output of the battery, P_{α} and P_{β} referring to the power of the left and right power arms, respectively, and P_{load} representing the load of the TPSS. Firstly, it is necessary to obtain the actual measured values of voltage and current for both power arms and calculate the power values P_{α} and P_{β}. Considering that the RPC is capable of controlling power flow between the two power arms, the combined power of the two arms, $P_{\mathrm{load}} = P_{\alpha} + P_{\beta}$, can be used to determine the operating mode.

Mode one: When the PV output is greater than the load of the TPSS, that is, $P_{\mathrm{pv}} > P_{\mathrm{load}}$, and the SOC of the battery is lower than its upper limit, the primary source of electricity for the TPSS is provided by the PV system. Meanwhile, any surplus electricity is stored in the battery.

Mode two: When the PV output is greater than the load of the TPSS, that is, $P_{\mathrm{pv}} > P_{\mathrm{load}}$, and the SOC of the battery reaches its upper limit, the primary source of electricity for the TPSS is provided by the PV system. However, any surplus electricity is discarded.

Mode three: When the PV output is less than the load of the TPSS, that is, $P_{\mathrm{pv}} < P_{\mathrm{load}}$, and the SOC of the battery has not reached its lower limit, the primary source of electricity for the TPSS is provided by the PV system. In case of shortfall, the battery is discharged and electricity is also obtained from the grid as a supplementary source.

Mode four: When the PV output is less than the load of the TPSS, that is, $P_{\mathrm{pv}} < P_{\mathrm{load}}$, and the SOC of the battery reaches its lower limit, the primary source of electricity for the TPSS is provided by the PV system. For any shortfall, electricity is purchased from the grid as a supplementary source.

The above-mentioned operating modes are illustrated in a flowchart shown in Fig. 2.

3. Mathematical model for optimal sizing and configuration

This paper employs a bilevel optimization model to make a configuration regarding ESS power capacity while conducting an optimization analysis of the operational mode of the TPSS under ESS services. The decision-making process for ESS capacity and power configuration needs to be comprehensively based on the actual measured PV generation and TPSS load. This is done with the objective of achieving the optimal ESS capacity and power while minimizing the annual operational costs of the ESS. Furthermore, the paper aims to solve optimization problems related to the operation of the TPSS, such as energy exchange with the ESS, under the provision of ESS services. In the proposed algorithm of this paper, the upper-level model is used to find the optimal PV consumption rate and solve the ESS configuration problem. The lower-level model, built upon the upper-level model, utilizes the consumption rate determined by the upper-level model and the ESS configuration to solve the system's optimization problem for operation.

Considering the inherent uncertainty of PV output, it is difficult to ensure its complete consumption in actual system operation. Therefore, configuring the ESS based solely on the assumption of complete consumption of PV power may not provide strong guidance for practical system operation. To fully utilize the function of the ESS in absorbing PV power, blind aiming for complete consumption may not be optimal. Instead, it is recommended to set a certain level of curtailment while ensuring partial consumption, allowing distributed PV energy sources to reasonably curtail excess power within a certain range. This approach will help achieve a more efficient utilization of the ESS in conjunction with PV generation.

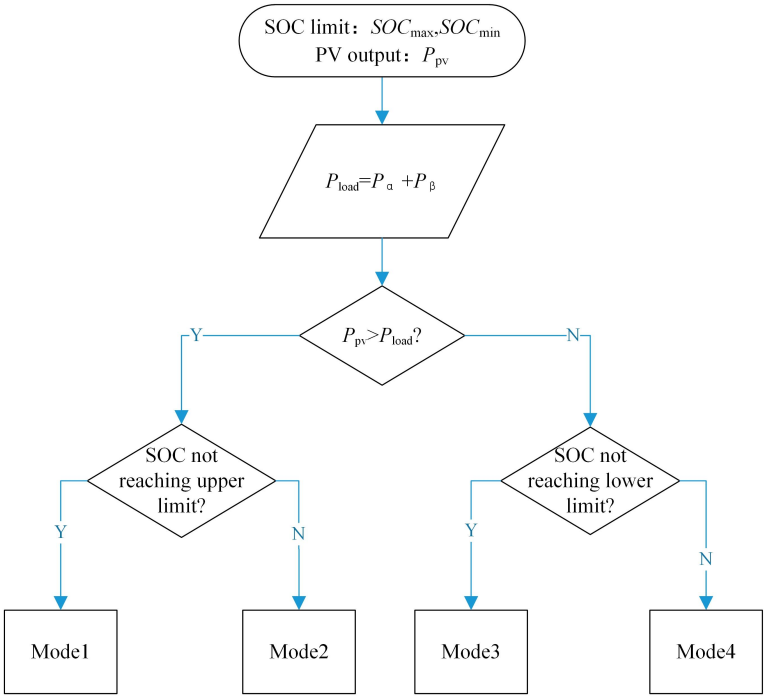

Fig. 2. Operating mode flowchart

3.1. Upper-level model

The upper-level model is used to solve the ESS configuration problem with the objective of minimizing the cost of the PV-ESS. The decision variable in this model is the power capacity of the ESS.

3.1.1. Objective function

The total cost of the ESS integration into the TPSS consists of the investment cost of the ESS plant and the electricity purchase cost from the grid by the TPSS. The optimization objective function can be represented as:

$$\min C_1 = C_{\text{inv}} + C_{\text{grid}}, \tag{1}$$

where C_{inv} is the investment and operational cost of the ESS, while C_{grid} is the annual cost of purchasing electricity from the grid for the TPSS.

3.1.1.1. Investment and operational cost of the ESS

The investment in the ESS includes both one-time construction costs and annual fixed investment costs for maintenance. When calculating the cost of ESS investment, it is important to consider the time value of money. Therefore, the investment construction cost can be expressed as follows:

$$C_{\text{inv}} = \frac{r(1+r)^m}{(1+r)^m - 1}(Q_{\text{P}}P_{\text{ESS}} + Q_{\text{E}}E_{\text{ESS}}) + Q_{\text{M}}P_{\text{ESS}}, \tag{2}$$

where r is the discount rate, m is the lifecycle of the device, P_{ESS} and E_{ESS} are the rated power and capacity of the ESS, Q_{P} is the unit power investment cost; Q_{E} is the unit capacity investment cost; Q_{M} is the unit power maintenance cost.

3.1.1.2. Electricity purchase cost from the grid by the TPSS

$$C_{\mathrm{grid}} = \sum_{i=1}^{T} \alpha(t) P_{\mathrm{grid}}(t), \tag{3}$$

where T is the scheduling period, $\alpha(t)$ is the time-of-use electricity price in each scheduling period, and $P_{\mathrm{grid}}(t)$ is the power purchased from the grid by the TPSS in each scheduling period.

3.1.2. Constraint conditions

3.1.2.1. ESS rate constraint

The rated capacity of the ESS is directly proportional to its rated power:

$$E_{\mathrm{ESS}} = \beta P_{\mathrm{ESS}}, \tag{4}$$

where β is the ESS energy ratio.

3.1.2.2. ESS charging and discharging constraint

During the same scheduling period, the charging and discharging state of the ESS is determined by the total energy demand after energy exchange at the point of common coupling. At the same time, it is restricted that the ESS cannot be charged and discharged simultaneously within the same scheduling period. The constraint conditions are as follows:

$$\begin{cases} P_{\mathrm{d}}(t) - P_{\mathrm{c}}(t) = P_{\mathrm{dESS}}(t) - P_{\mathrm{cESS}}(t) \\ 0 \le P_{\mathrm{cESS}}(t) \le \xi_1(t) P_{\mathrm{ESS}} \\ 0 \le P_{\mathrm{dESS}} \le \xi_2(t) P_{\mathrm{ESS}} \end{cases}, \tag{5}$$

where $P_{\mathrm{c}}(t)$ and $P_{\mathrm{d}}(t)$ are the charging and discharging power from the TPSS to the ESS in each scheduling period, respectively, $P_{\mathrm{cESS}}(t)$ and $P_{\mathrm{dESS}}(t)$ are the charging and discharging power of the ESS in each scheduling period, respectively, $\xi_1(t)$ and $\xi_2(t)$ are the charging and discharging indicators of the ESS in the t scheduling period.

3.1.2.3. ESS SOC constraint

The initial and final state of ESS's SOC should be kept equal:

$$\begin{cases} \mathrm{SOC}(t) = \mathrm{SOC}(t-1) + \eta_1 P_{\mathrm{cha}}(t) - \frac{1}{\eta_2} P_{\mathrm{dis}}(t) \\ \mathrm{SOC}_{\min} \le \mathrm{SOC}(t) \le \mathrm{SOC}_{\max} \\ \mathrm{SOC}_{\mathrm{initial}} = \mathrm{SOC}_{\mathrm{final}} \\ \xi_1(t) + \xi_2(t) \le 1 \end{cases}, \tag{6}$$

where η_1 and η_2 are the charging and discharging efficiency of the ESS, respectively, while $\mathrm{SOC}_{\max}$ and $\mathrm{SOC}_{\min}$ are the upper and lower limits of the SOC of the ESS.

3.2. Lower-level model

The lower-level model is used to solve the system's economic operation problem, with the optimization objective of minimizing the annual operating cost of the TPSS. The decision variables include the operating conditions of various equipment, the electricity purchasing situation of the TPSS from the grid, the power exchange between the TPSS and the ESS, and the PV power consumption rate.

3.2.1. Objective function

The optimization objective of the lower-level model is to minimize the annual operating cost of the TPSS, which can be represented as follows:

$$\min C_2 = C_{\text{grid}} - C_{\text{cESS}} + C_{\text{dESS}} + C_{\text{serv}}, \tag{7}$$

where C_{cESS} represents the benefits of charging the ESS from the TPSS; C_{dESS} is the cost of discharging the ESS to the TPSS; C_{serv} is the annual service cost payment from the TPSS to the ESS.

3.2.1.1. Benefits of charging the ESS from the TPSS

$$C_{\text{cESS}} = \lambda_1(t)P_{\text{c}}(t), \tag{8}$$

where $\lambda_1(t)$ is the time-of-use electricity price for charging the ESS from the TPSS in different dispatch periods.

3.2.1.2. Cost of discharging the ESS to the TPSS

$$C_{\text{dESS}} = \lambda_2(t)P_{\text{d}}(t), \tag{9}$$

where $\lambda_2(t)$ is the time-of-use electricity price for discharging the ESS in different dispatch periods.

3.2.1.3. Annual service cost payment from the TPSS to the ESS

$$C_{\text{serv}} = Q_{\text{S}}(P_{\text{c}}(t) + P_{\text{d}}(t)), \tag{10}$$

where Q_S is the service cost of power per unit for the TPSS to pay to the ESS.

3.2.2. Constraint conditions

3.2.2.1. Power balance constraint

$$P_{\text{pv}}(t) + P_{\text{grid}}(t) + P_{\text{dESS}}(t) = P_{\text{load}}(t) + P_{\text{cESS}}(t), \tag{11}$$

where $P_{\text{pv}}(t)$ is the output of PV power in each scheduling period, and $P_{\text{load}}(t)$ is the TPSS load in each scheduling period.

3.2.2.2. Energy exchange constraint

The TPSS is capable of engaging in energy exchange with the ESS, while ensuring that charging and discharging operations do not occur simultaneously within a given scheduling period. Furthermore, the energy exchange constraint is subject to the power constraints imposed on the

charging and discharging processes of the ESS. This energy exchange constraint can be formulated as follows:

$$\begin{cases} P_{\mathrm{d}}(t) - P_{\mathrm{c}}(t) = P_{\mathrm{dESS}}(t) - P_{\mathrm{cESS}}(t) \\ 0 \le P_{\mathrm{c}}(t) \le \xi_3(t) P_{\mathrm{ESS.max}} \\ 0 \le P_{\mathrm{d}}(t) \le \xi_4(t) P_{\mathrm{ESS.max}} \\ \xi_3(t) + \xi_3(t) \le 1 \\ 0 \le P_{\mathrm{c}}(t) \le P_{\mathrm{ESS}} \\ 0 \le P_{\mathrm{c}}(t) \le P_{\mathrm{ESS}} \end{cases}, \tag{12}$$

where $P_{\mathrm{ESS.max}}(t)$ is the maximum power exchange between the TPSS and the ESS. $\xi_3(t)$ and $\xi_4(t)$ are the charging and discharging indicators for the system during the t scheduling period.

The power purchased by the TPSS from the grid needs to satisfy certain limiting conditions, which can be represented as follows:

$$0 \le P_{\mathrm{grid}}(t) \le P_{\mathrm{grid.max}}(t), \tag{13}$$

where $P_{\mathrm{grid.max}}(t)$ is the maximum power purchased by the TPSS from the grid.

3.2.2.3. PV consumption constraint

$$\begin{cases} \sum_{t=1}^{T} P_{\mathrm{pv}}(t) = \lambda \sum_{t=1}^{T} P_{\mathrm{pv.max}}(t) \\ 0 \le P_{\mathrm{pv}}(t) \le P_{\mathrm{pv.max}}(t) \end{cases}, \tag{14}$$

where $P_{\mathrm{pv.max}}(t)$ is the maximum output of PV during scheduling period t, and λ represents the annual PV consumption rate.

3.2.2.4. RPC power constraint

During the operation of the system, at each moment, the transmission power should not exceed the maximum limit of RPC transmission power, which can be represented as follows:

$$|P_{\mathrm{trans}}(t)| \le |P_{\mathrm{trans.lim}}(t)|, \tag{15}$$

where $P_{\mathrm{trans}}(t)$ is the maximum transmission power of the RPC during scheduling period t.

4. Case study

4.1. Solution methods

In the bilevel optimization model proposed in this paper, there are non-linear constraints and the two-level models are coupled, making it difficult to solve directly. The Karush–Kuhn–Tucker (KKT) method can be used to transform and solve the model [22]. This method, under the assumption that the lower-level model is convex, continuous, and differentiable, transforms the lower-level model into an additional constraint condition for the upper-level model using the complementary relaxation conditions of the lower-level model. This results in a single-level model where the optimized objective only contains the original upper-level model's objective, and the

original lower-level model's optimized objective and constraints exist in constrained form. By using the KKT function in the YALMIP toolbox, the KKT conditions of the lower-level optimization can be directly solved and used as constraints for the upper-level optimization, forming a single-level mixed-integer linear programming model. Subsequently, a commercial solver such as CPLEX can be invoked in MATLAB to solve the model.

4.2. Data configuration

This study focuses on the power generation data of a 60 MW PV power station in Northwestern China and the daily measured data of a traction substation in Northwestern China. The study divides a day into 24 scheduling intervals, with each interval lasting for 1 hour. Due to relevant policies, the TPSS is not allowed to feed electricity back into the grid. The TPSS purchases electricity from the grid using the time-of-use electricity pricing for large industrial consumers in a certain province in Northwestern China. The PV power generation, TPSS load, and time-of-use electricity price are shown in Fig. 3:

To analyze the impact of the PV consumption rate on the economic operation of the system, the following cases are set up for comparative analysis:

Case 1: Solving the PV consumption rate and system operating costs under the constraints described in this paper.

Case 2: Setting the PV consumption rate to 100% and obtaining the system operating costs.

In the case study, case 1 utilizes the bilevel optimization method proposed in this paper for solving. Case 2 is similar to case 1, but the PV consumption rate is forcibly set to 100%. The other basic parameters of this paper are shown in Table 1.

Table 1. Parameter configuration

Parameter name	**Symbol**	**Value**	**Unit**
Discount rate	r	0.03	1
Lifecycle of the device	m	20	Year
Unit power investment cost	Q_{P}	683.4	USD/MW
Unit capacity investment cost	Q_C	1 093.4	USD/MW
Unit power maintenance cost	Q_{M}	13.7	USD/MW
Unit power service cost	Q_S	109.3	USD/MW
SOC upper limit	$\mathrm{SOC}_{\max}$	90	%
SOC lower limit	$\mathrm{SOC}_{\min}$	20	%
Initial SOC	$\mathrm{SOC}_{\mathrm{initial}}$	30	%
Maximum power purchase from the grid	$P_{\mathrm{grid.\,max}}$	19	MW
Maximum limit of RPC transmission power	$P_{\mathrm{trans.lim}}$	40	MW

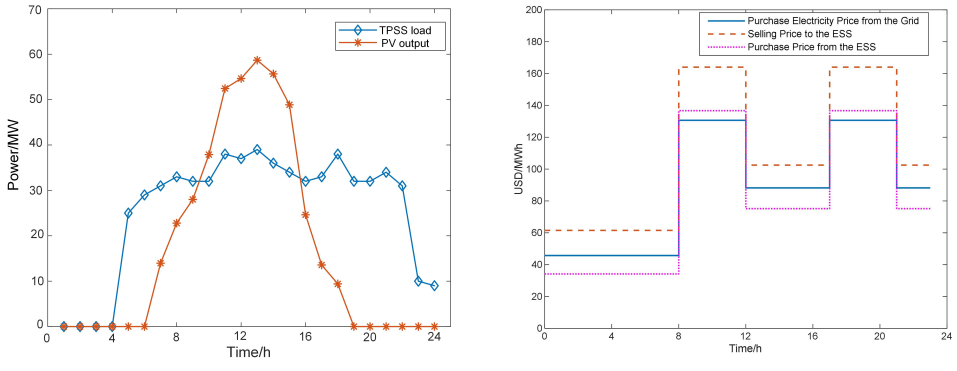

(a) (b)

Fig. 3. PV output and TPSS load (a); time of use electricity price (b)

4.3. Case study

In case 1, the solution yields a configured ESS power of 79.0359 MW, a configured capacity of 158.0718 MWh, and a PV consumption rate of 96.8749%. The power balance situation for case 1 is illustrated in Fig. 4(a).

Based on the analysis of the power balance situation, the system experiences a certain amount of curtailed solar energy only at 12 h, resulting in a high overall consumption rate. During instances of inadequate PV output, the TPSS necessitates the procurement of a substantial quantity of electrical power from the grid. The SOC curve and the charging/discharging status of the ESS in case 1 are depicted in Fig. 4(b).

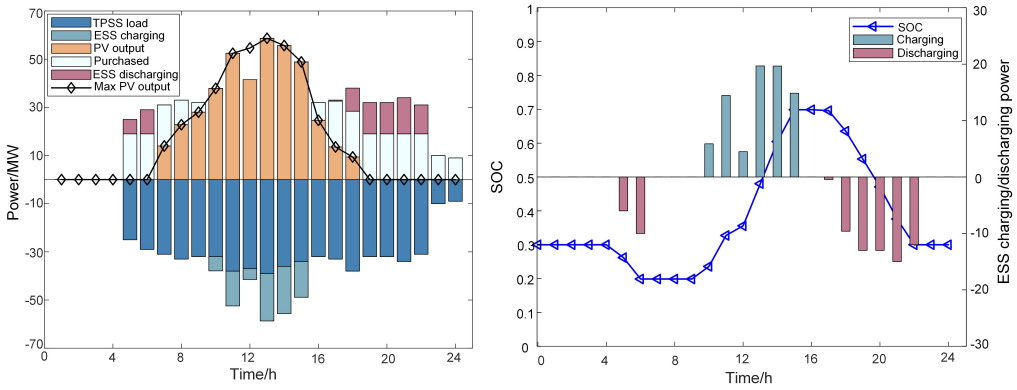

(a) (b)

Fig. 4. Power balance of case 1 (a); SOC of ESS (b)

Referring to Fig. 4(b), the ESS does not engage in any charging or discharging activities within the time intervals of 0–4 h, 6–9 h, 15–17 h, and 22–24 h. Charging and discharging events transpire during the remaining periods, promoting energy exchange within the system and effectuating energy transfer across temporal scales. Set the PV consumption rate to 100% and solve case 2, the power balance and SOC curve under case 2 are shown in Fig. 5.

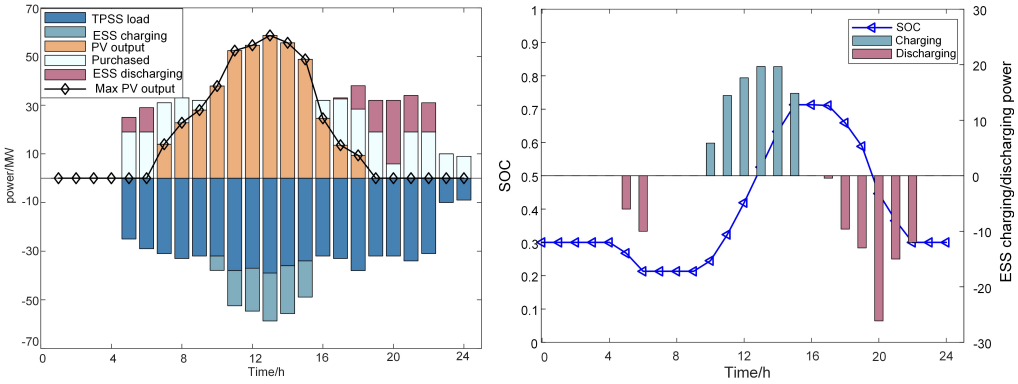

(a) (b)

Fig. 5. Power balance of case 2(a); SOC of ESS (b)

Based on Fig. 5(a), all PV energy is fully consumed. The designed ESS power obtained in case 2 is 92.1776 MW, with a configured capacity of 184.3552 MWh. In comparison to case 2, the capacity configuration of the ESS decreased by approximately 13.14% in case 1.

The comparison of the operational costs and benefits between case 1 and case 2 is presented in Table 2 below:

Table 2. Cost-benefit comparison

Name	Case 1	Case 2	Unit
Benefits of ESS	18 448.8028	21 486.1496	USD
Total operational cost of TPSS	54 924.2812	58 625.6544	USD
Overall operational cost of TPSS	36 484.5222	37 165.0407	USD

As indicated in Table 2, while case 2 ensures full utilization of PV energy, the concurrent incorporation of additional ESS devices leads to an overall rise in system operational expenses, consequently reducing its economic efficacy.

The comparison of system operating costs at different PV consumption rates is as shown in Fig. 6(a). Simultaneously, to examine the possibility of an optimal solution with a lower PV consumption rate, the overall operational cost of the TPSS was computed for PV consumption rates ranging from 0% to 100%. The findings are depicted in Fig. 6(b).

Based on the results obtained, it was observed that the optimal PV consumption rate for this study is 96.8749%. At this rate, the overall operational cost of the TPSS is minimized. The overall operational cost of the TPSS shows an increasing trend when the PV consumption rate is below the optimal value. When the PV consumption rate exceeds the optimal value, the configured capacity of the ESS increases, resulting in higher costs.

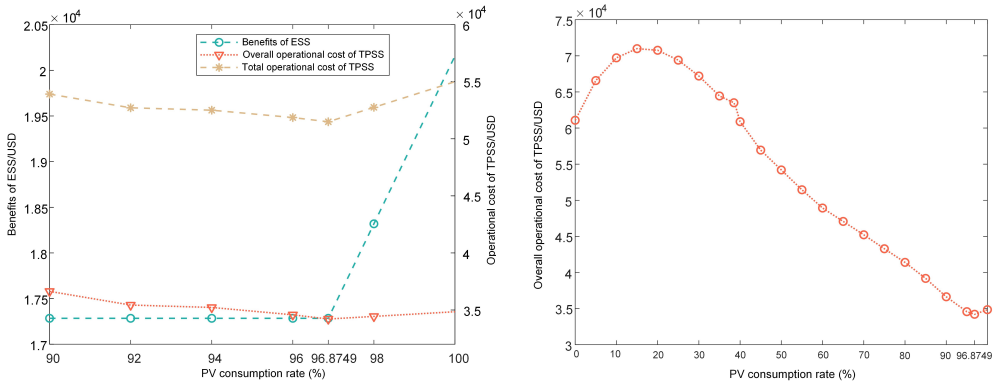

(a) (b)

Fig. 6. Comparison of operational costs at different PV consumption rates (a); the overall operational cost of TPSS at different PV consumption rates (b)

5. Conclusions

By integrating the ESS with PV into the TPSS, the study promotes the local consumption of PV energy, leading to reduced operational costs of the TPSS. The study reveals that the optimal PV consumption rate is 96.8749%, which results in a decrease in ESS capacity by approximately 13.14% compared to a 100% PV consumption rate. These findings demonstrate that the proposed bilevel optimization model algorithm effectively addresses multi-objective optimization problems by determining the optimal ESS capacity and calculating the optimal PV consumption rate, ultimately minimizing the operating costs of the TPSS. In prospective research, contemplation can be directed to the integration of energy storage devices, such as supercapacitors, along with batteries, established upon the foundation of this article, thereby forming a hybrid energy storage system (HESS). By capitalizing on the benefits of various energy storage technologies, it is possible to explore more efficient management and utilization of energy.

Acknowledgements

This work is supported by the Regional Project of National Natural Science Foundation of China (No. 52367009, No. 52067013); the Natural Science Key Foundation of Science and Technology Department of Gansu Province (21JR7RA280, 22JR5RA318, 22JR5RA353 22JR11RA162).

References

[1] https://www.mot.gov.cn/fenxigongbao/hangyegongbao/202305/P020230530535262349964.pdf, accessed August 2023.

[2] Haghighatseresht A., MansouriBidekani R., Razavi S. *et al.*, *Investigating the impact of building local photovoltaic power plants on the national grid, an artificial intelligence approach*, Ain Shams Engineering Journal, vol. 14, no. 11, 102518 (2023), DOI: 10.1016/j.asej.2023.102518.

[3] Mirjalili M.A., Aslani A., Zahedi R. *et al.*, *A comparative study of machine learning and deep learning methods for energy balance prediction in a hybrid building-renewable energy system*, Sustainable Energy Research, vol. 10, no. 8 (2023), DOI: 10.1186/s40807-023-00078-9.

[4] Pourrahmani H., Zahedi R., Daneshgar S. *et al.*, *Lab-scale investigation of the integrated backup/storage system for wind turbines using alkaline electrolyzer*, Energies, vol. 16, no. 9, 3761 (2023), DOI: 10.3390/en16093761.

[5] Khah M.V., Zahedi R., Eskandarpanah R. *et al.*, *Optimal sizing of residential photovoltaic and battery system connected to the power grid based on the cost of energy and peak load*, Heliyon, vol. 9, no. 3, e14414 (2023), DOI: 10.1016/j.heliyon.2023.e14414.

[6] Deng W., Dai C., Chen W., *Application of PV Generation in AC/DC Traction Power Supply System and the Key Problem Analysis under the Background of Rail Transit Energy Internet*, Proceedings of the Chinese Society of Electrical Engineering, vol. 39, no. 19, pp. 5692–5702(2019), DOI: 10.13334/j.0258-8013.pcsee.181848.

[7] Chen W., Wang X., Li Q., Han Y., Wang W., *Review on the Development Status of PV Power Station Accessing to Traction Power Supply System for Rail Transit*, Power System Technology, vol. 43, no. 10, pp. 3663–3670 (2019), DOI: 10.13335/j.1000-3673.pst.2018.2498.

[8] Méndez-Hernández Y., Müggenburg E., Lynass M. *et al.*, *Design aspects for high voltage MW PV systems for railway power supply*, Proceedings of the 29th European Photovoltaic Solar Energy Conference and Exhibition, Amsterdam (2014), https://www.researchgate.net/profile/Yaru-Hernandez/publication/270876054_Design_Aspects_for_High_Voltage_MW_PV_Systems_for_Railway_Power_Supply/links/56b2102908aed7ba3fedb391/Design-Aspects-for-High-Voltage-MW-PV-Systems-for-Railway-Power-Supply.pdf.

[9] Hayashiya H. *et al.*, *Potentials, peculiarities and prospects of solar power generation on the railway premises*, 2012 International Conference on Renewable Energy Research and Applications (ICRERA), Nagasaki, Japan, pp. 1–6 (2012), DOI: 10.1109/ICRERA.2012.6477458.

[10] D'Arco S., Piegari L., Tricoli P., *Comparative Analysis of Topologies to Integrate Photovoltaic Sources in the Feeder Stations of AC Railways*, IEEE Transactions on Transportation Electrification, vol. 4, no. 4, pp. 951–960 (2018), DOI: 10.1109/TTE.2018.2867279.

[11] Wu C.-P., Luo A., Xu X.-Y., Ma F.-J., Sun J., *Integrative compensation method of negative phase sequence and harmonic for high-speed railway traction supply system with V/v transformer*, Proceedings of the Chinese Society of Electrical Engineering, vol. 30, no. 16, pp. 111–117 (2010), DOI: 10.13334/j.0258-8013.pcsee.2010.16.014.

[12] Roudsari H.M., Jalilian A., Jamali S., *Flexible Fractional Compensating Mode for Railway Static Power Conditioner in a V/v Traction Power Supply System*, IEEE Transactions on Industrial Electronics, vol. 65, no. 10, pp. 7963–7974 (2018), DOI: 10.1109/TIE.2018.2801779.

[13] Zhao X., Xie Z., Wang Y., Chen X., Xin Y., Mu X., *Low-frequency Stability Analysis of Photovoltaic Connected Traction Power Supply System Based on Extended Forbidden Region-based Criterion*, High Voltage Engineering, vol. 49, no. 5, pp. 1997–2007 (2023), DOI: 10.13336/j.1003-6520.hve.20220690.

[14] Wang Y., He Y., Chen X., Zhao M., Xie J., *A layered compensation optimization strategy of energy storage type railway power conditioner*, Archives of Electrical Engineering, vol. 71, no. 1, pp. 5–20 (2022), DOI: 10.24425/aee.2022.140194.

[15] Wang Ying, Yang H., Chen X. *et al.*, *Train based on virtual synchronous generator technology uninterrupted phase-separation passing study*, Archives of Electrical Engineering, vol. 72, no. 3, pp. 755–768 (2023), DOI: 10.24425/aee.2023.146048.

[16] Deng W., Dai C., Chen W., Zhang H., *Research Progress of Railway Power Conditioner*, Proceedings of the Chinese Society of Electrical Engineering, vol. 40, no. 14, pp. 4640–4655 (2020), DOI: 10.13334/j.0258-8013.pcsee.191470.

[17] Chengpeng X., Ying H., Qi L. *et al.*, *Research on coordinated control method of PV and battery access traction power supply system based on RPC*, 2020 IEEE Sustainable Power and Energy Conference (iSPEC), pp. 173–179 (2020), DOI: 10.1109/iSPEC50848.2020.9350956.

[18] Yuan J., Qu K., Zheng X., Min Y., *Optimizing Research on Hybrid Energy Storage System of High Speed Railway*, Transactions of China Electrotechnical Society, vol. 36, no. 19, pp. 4161–4169+4182 (2021), DOI: 10.19595/j.cnki.1000-6753.tces.201060.

[19] Zhang Y., Hu H., Geng A., Chen J., Ge Y., Wang K., *Capacity optimization configuration of hybrid energy storage system for electrified railway considering peak load shifting*, Electric Power Automation Equipment, vol. 43, no. 2, pp. 44–50 (2023), DOI: 10.16081/j.epae.202207012.

[20] Li X., Lu J., Xiao L., Jin Z., *Capacity Optimization Configuration of Hybrid Energy Storage System for Long Steep Slope of High-Speed Railway*, Transactions of China Electrotechnical Society, pp. 1–16 (2023), DOI: 10.19595/j.cnki.1000-6753.tces.221199.

[21] Chen M., Liang Z., Cheng Z., Zhao J., Tian Z., *Optimal Scheduling of FTPSS with PV and HESS Considering the Online Degradation of Battery Capacity*, IEEE Transactions on Transportation Electrification, vol. 8, no. 1, pp. 936–947 (2022), DOI: 10.1109/TTE.2021.3093321.

[22] Sinha A., Soun T., Deb K., *Using Karush–Kuhn–Tucker proximity measure for solving bilevel optimization problems*, Swarm and Evolutionary Computation, vol. 44, pp. 496–510 (2019), DOI: 10.1016/j.swevo.2018.06.004.